Finding seed points for organ segmentation using example annotations

Ranveer Joyseeree[ab], Henning Müller[ac]

[a]University of Applied Sciences Western Switzerland (HES–SO), Sierre, Switzerland;
[b]Eidgenössische Technische Hochschule (ETH), Zürich, Switzerland;
[c]Medical Informatics, University Hospitals & University of Geneva, Switzerland;

ABSTRACT

Organ segmentation is important in diagnostic medicine to make current decision–support tools more effective and efficient. Performing it automatically can save time and labor. In this paper, a method to perform automatic identification of seed points for the segmentation of organs in three–dimensional (3D) non–annotated, full–body magnetic resonance (MR) and computed tomography (CT) volumes is presented. It uses 3D MR and CT acquisitions along with corresponding organ annotations from the Visual Concept Extraction Challenge in Radiology (VISCERAL) banchmark.

A training MR or CT volume is first registered affinely with a carefully–chosen reference volume. The registration transform obtained is then used to warp the annotations accompanying that training volume. The process is repeated for several other training volumes. For each organ of interest, an overlap volume is created by merging the warped training annotations corresponding to it. Next, a 3D probability map for organ location on the reference volume is derived from each overlap volume. The centroid of each probability map is determined and it represents a suitable seed point for segmentation of each organ.

Afterwards, the reference volume can be affinely mapped onto any non–annotated volume and the mapping applied to the pre–computed volume containing the centroid and the probability distribution for an organ of interest. Segmentation on the non–annotated volume may then be started using existing region–growing segmentation algorithms with the warped centroid as the seed point and the warped probability distribution as an aid to the stopping criterion. The approach yields very promising results.

Keywords: medical image processing, 3D probability maps, automatic seed point detection

1. INTRODUCTION

Medical imaging has revolutionized clinical care since its advent. Clinicians are now able to gather information regarding the state of a patient's inner anatomy without the need for invasive approaches. In fact, medical doctors have come to rely very heavily on imaging for diagnosis and pre–operative surgical planning.[1] As a result, medical information is being produced and collected at such a massive rate that there is a clear need for a strategy in relation to its efficient processing and storage.[2] This is especially important if one wants to exploit the great wealth of information contained in images gathered for past clinical cases in order to improve diagnosis and surgical planning outcomes.

Automating the processing and efficient storage of the huge quantities of data being collected is becoming vital. However, automation requires that algorithms understand the content of images. In this paper, a method to automatically process the contents of full–body MR/CT scans in order to find seed points that can be used for organ segmentation and subsequent identification is proposed. In the segmentation case, automation will greatly reduce the burden on clinicians who are called upon for manual delineation of organs in full–body scans. They will, thus, save time which they can invest in other aspects of their work in order to provide better service to patients. As for automatic organ identification, it will be very useful in the semi–automatic generation of descriptive reports, in line with the idea of DICOM structured reporting.[?,?]

Further author information: (Send correspondence to Henning Müller, Email: henning.mueller@hevs.ch)

In addition, this study is well aligned with the FP7 VISCERAL[3] benchmark* which involves achieving automatic segmentation of anatomical structures in non–annotated full–body MR and CT volumes. The project also involves the identification of a 'surprise' organ for which training data needs to be analyzed without knowing the organ in advance. Only training data and no a–priori knowledge can thus be used. A segmentation method that uses the proposed method of seed point identification would be perfectly suited to achieve the goals of VISCERAL.

2. METHODS

A full–body MR or CT volume, labelled as X, is chosen from the database of training acquisitions, Y_1 to Y_N (where N is the size of the database), provided for VISCERAL. Each acquisition has been examined by expert radiologists who have annotated up to 20 different organs and saved each annotation, labelled A(Y_n,organ) (where n is the identifier of a particular volume in the database), as a separate volume. Care is taken such that X is not an outlier in terms of body shape and size. This ensures that the error introduced by affine registration, which will be used in the next step, is kept to a minimum. Figure 1 illustrates the choice of X for this paper and includes an illustrative annotation, $A(X$,liver), which is displayed as a white region with horizontal stripes.

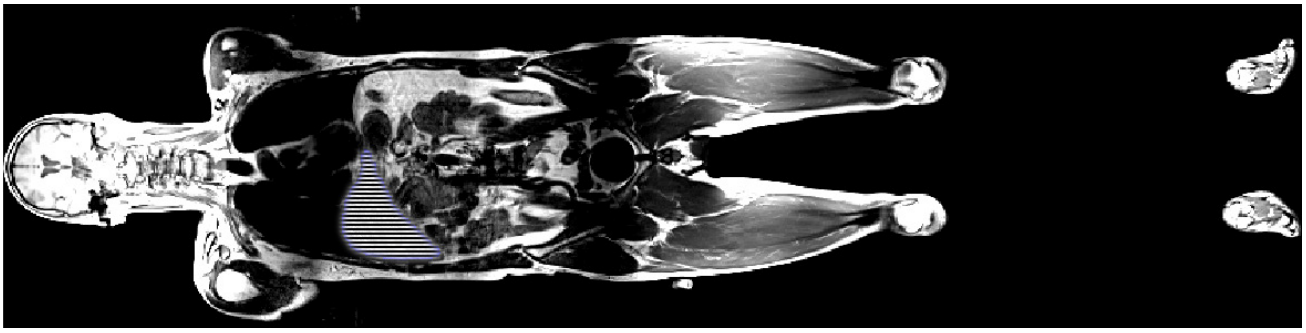

Figure 1: A full–body MR volume is chosen as X. For illustrative purposes, X is superimposed with the liver annotation, shown as a white region with horizontal stripes: $A(X$,liver)

2.1. Registration

A training volume, labelled as Y_1, is then registered with X. Y_1 is chosen as the moving volume and X is the fixed volume. An affine transformation[4] is applied during the registration process as it offers a good compromise between computation speed and accuracy. The cost metric used is mutual information (MI)[5] as two modalities — MR and CT — may need to be registered together. To speed up the computation of MI, the implementation by Mattes et al.[6,7] is utilized. To minimize the interpolation errors that necessarily occur during registration while keeping computation time low, B–Spline interpolation[8–10] is carried out. After the successful completion of registration, the linear transform T that maps Y_1 onto X is obtained. Next, one organ of interest, Z, is picked. The annotation volume, A(Y_1,Z), is then converted into a binary volume before being transformed using T, giving $A^T(Y_1, Z)$. The latter is resampled such that it has the exact volume and voxel dimensions as $A(X, Z)$, which itself has the same mensurations as X.

2.2. Creation of probability distribution volume

To create a probability distribution volume, the above registration step is carried out for all N available VISCERAL volumes. For each training volume Y_n, a different transformation T and a different warped annotated volume $A^T(Y_n, Z)$ are obtained. Since $A^T(Y_n, Z)$ for all n have the same volume and voxel sizes as $A(X, Z)$, they may be combined together voxel–wise and then normalized according to equation (1) to obtain the probability

*VISCERAL benchmark: http://www.visceral.eu/benchmark-1/, 2012. [Online; accessed 15-January-2014].

distribution volume for organ Z: PD_Z. Please note that $A(X, Z)$ is excluded from the above calculation in order to avoid bias.

$$PD_Z = \frac{1}{N} \sum_{n=1}^{N} A^T(Y_n, Z) \tag{1}$$

2.3. Generation of a seed point

The centroid of PD_Z, represented in row vector form as $\begin{bmatrix} x_c & y_c & z_c \end{bmatrix}$, corresponds to the weighted average location of a point that lies within PD_Z. For an MxNxP volume, it can be found using equation (2), where $V(x, y, z)$ is the voxel value at coordinates (x, y, z), which is represented as $\begin{bmatrix} x & y & z \end{bmatrix}$ in vector form. For a volume, B, on which the seed point for segmentation has to be found, affine registration between X and B is carried out. This time, X is used as the moving image while B is the fixed volume. The obtained transformation is applied to the volume containing the centroid found above. The location of the warped centroid may now be used as a seed point for segmentation on volume B.

$$\begin{bmatrix} x_c & y_c & z_c \end{bmatrix} = \frac{\sum_{x=1}^{M} \sum_{y=1}^{N} \sum_{z=1}^{P} V(x, y, z) * \begin{bmatrix} x & y & z \end{bmatrix}}{\sum_{x=1}^{M} \sum_{y=1}^{N} \sum_{z=1}^{P} V(x, y, z)} \tag{2}$$

2.4. Region–growing algorithm for segmentation

Once, the seed point for segmentation, C', is determined, its neighbouring voxels are assessed in order to determine if they belong to the region that C' lies in. If a neighbouring voxel is deemed to lie in that region, it becomes a new seed point and its neighbourhood is assessed likewise. The process continues recursively until no more voxels lying in the region are found.

In this paper, a simple set of criteria are used to assess whether a voxel, V, lies on the same organ as C'. They are as follows:

1. V must lie within $PD_{Z'}$.
2. V must have a gray value between a lower threshold Th_L and an upper threshold Th_H.

To find Th_L and Th_H, an analysis of the distribution of voxel intensity values within the organ of interest and in its immediate vicinity is required. To maximize the separation between the distribution curve of the organ voxel intensity values and that of the neighbouring voxel intensity values, histogram equalization[11] is carried out on the volume under analysis and the resulting volume is subjected to anisotropic diffusion.[12] Histogram equalization enhances the contrast between different tissue types in the volume and anisotropic diffusion smoothes out the noise in it while maintaning the sharpness of edges. Th_L and Th_H are the optimal values of voxel intensity that minimize the number of voxels mislabelled in the segmentation process.

2.5. Evaluation of segmentation

The effectiveness of the segmentation algorithm presented, and, therefore, the effectiveness of the proposed method to find seed points for segmentation, may be assessed using Dice's coefficient[13] according to equation 3. The computed segmented region, D, may be compared to a segmented region, E, delineated by an expert on the same volume. $|D|$ refers to the total number of voxels in D while $|D \cap E|$ refers to the total number of overlapping voxels of D and E.

$$Dice(D, E) = \frac{2\,|D \cap E|}{|D| + |E|} \tag{3}$$

3. RESULTS

The method above is applied to a series of MR and CT volumes from the VISCERAL dataset. Figure 2a shows the computed probability distribution volume for the liver, PD_{liver}, in coronal view . The lightest region indicates a probability of one for a voxel to lie on the liver and the darkest region indicates a probability of zero. The visualisation was generated using 3D Slicer†.[14]

Figure 2b illustrates the centroid of PD_{liver} as a very dark point near the centre of the probability distribution. When the same procedure is applied to the right lung, right kidney and the urinary bladder, Figures 3–4 are obtained respectively. It may be observed that the seed points are located well within the target organs, implying that effective segmentation algorithms are expected to accurately segment those organs. To test how often that is the case, 7 specific volumes are chosen in turn as the reference volume and whether the calculated centroids fall within the corresponding expert annotations is investigated. The result of doing so is presented in Table 1. A zero indicates that the centroid falls outside the organ to be segmented, thereby leading to a segmentation failure. A value of 1, on the other hand, indicates that the centroid falls inside the organ to be segmented, thereby paving the way to a successful segmentation.

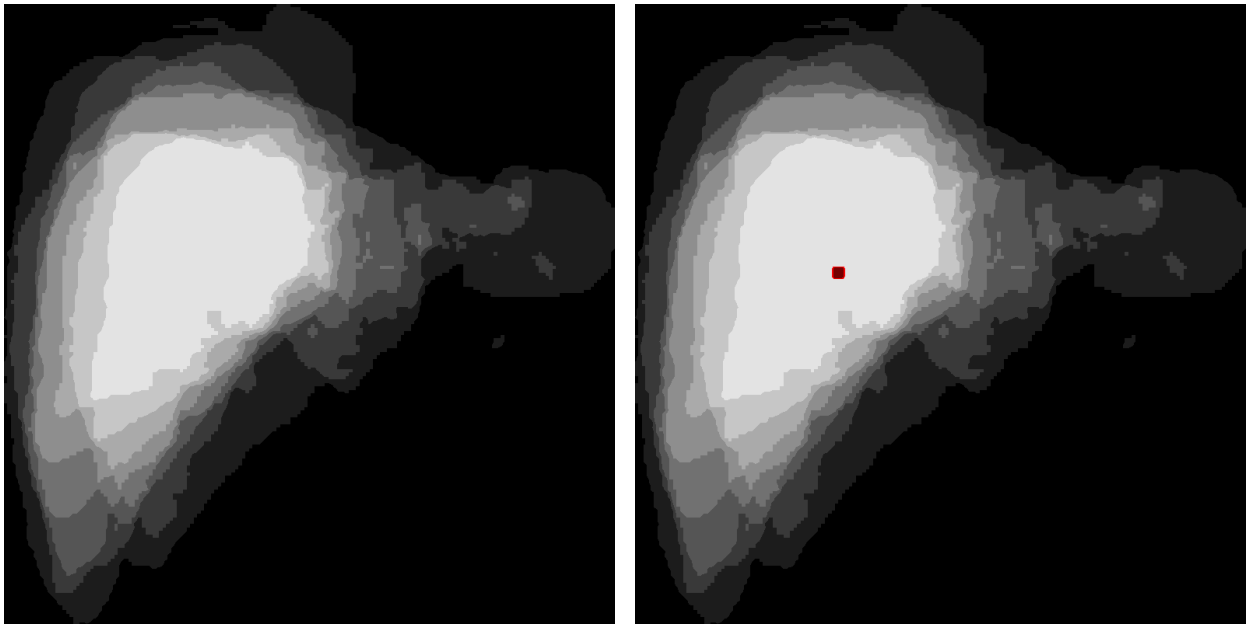

(a) (b)

Figure 2: (a) Probability distribution volume of the liver (coronal view), produced using 9 liver annotations. The lightest region indicates a probability of 1 for a voxel to lie on the liver and the darkest region indicates a probability of 0; (b) Centroid of the liver shown as the darkest point in the probability distribution volume.

†3D Slicer: http://www.slicer.org/, 2013. [Online; accessed 31-July-2013].

Figure 3: Encircled seed point superposed on X and PD_{liver}

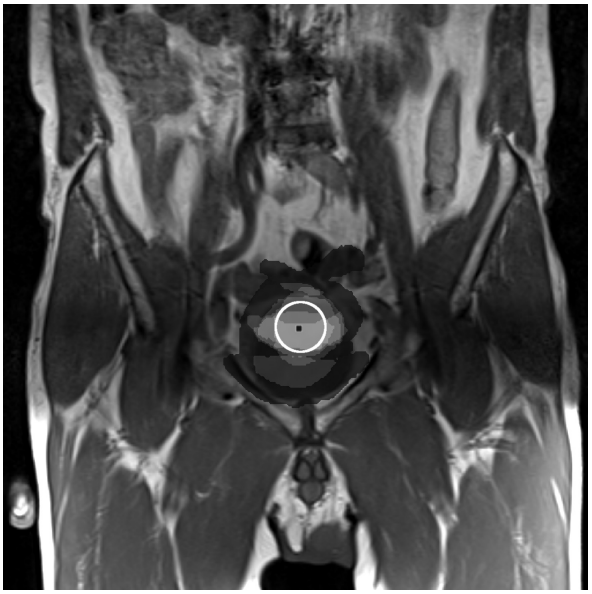

Figure 4: Encircled seed point on X and $PD_{urinary\_bladder}$

Figure 5: Encircled seed point superposed on X and PD_{left_lung}

Figure 6: Encircled seed point on X and PD_{left_kidney}

Patient ID	Liver	Spleen	Urinary bladder	Right lung	Left lung	Right kidney	Left kidney
10000104	0	0	1	1	1	1	1
10000105	1	1	1	0	0	1	1
10000106	1	1	1	1	1	1	1
10000108	1	1	0	1	1	1	1
10000109	1	1	0	1	1	1	1
10000110	1	0	0	1	1	1	1
10000111	1	1	0	1	1	1	1

Table 1: Shown here is the result of investigating whether calculated centroids that are subsequently used as segmentation seed points fall within the target organ on the reference image. A value of zero indicates that the centroid falls outside the target organ while a value of 1 indicates that it falls within it.

To provide an illustration of the merit of the proposed algorithm for finding seed points, a simple region–growing segmentation algorithm was implemented and an attempt was made to segment the liver, right lung and left lung from another set of 7 volumes as above using the obtained seed points.

For each of the three separate targets, thresholds Th_L and Th_H for region-growing segmentation have to be found. This is done by analyzing the distribution of voxel intensity values within and just outside the target organ. This process is illustrated for the liver by Figure 7. The solid line is the distribution of grayscale values within the liver for all the training volumes used to create the organ probability map while the dotted line is that for voxels in the neighbourhood of the liver in those training volumes. To minimize the segmentation error, the lower and upper thresholds are chosen at the points where the two distributions cross. That is done automatically in our algorithm.

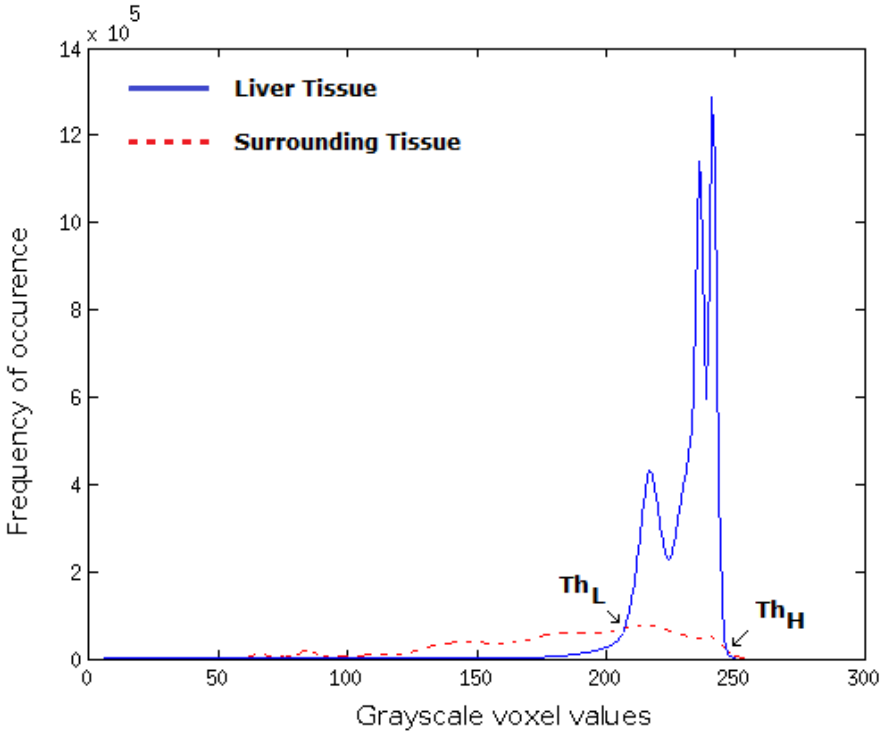

Figure 7: Shown with the solid line is the distribution of grayscale values for voxels marked as the liver in the training volumes. The distribution for voxels just outside the liver in the same volumes is shown as the dotted line.

After choosing the thresholds, region-growing segmentation is carried out using the seed points identified previously. The white segmented region in Figure 8 is obtained for the liver. Similarly, the white regions in Figure 9 and Figure 10 are obtained for the left lung and right lung respectively. The respective Dice's coefficient for each of the above segmentations are 0.884, 0.969, and 0.972.

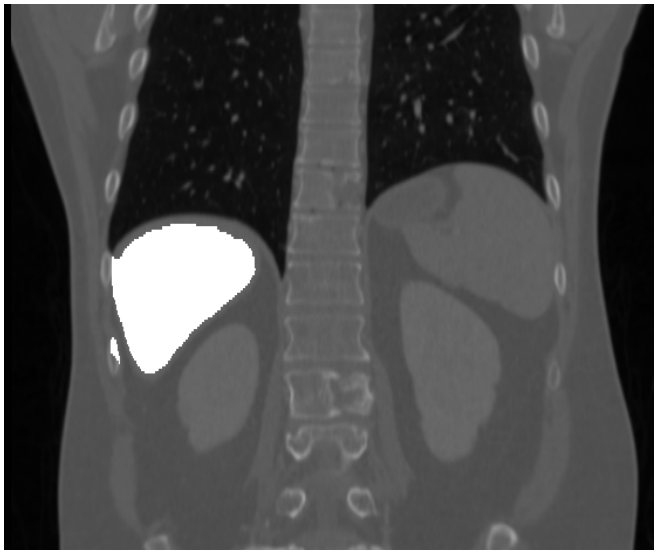

Figure 8: The result of running a simple region-growing segmentation algorithm using a computed liver seed point is shown as a white area superimposed on the volume under examination.

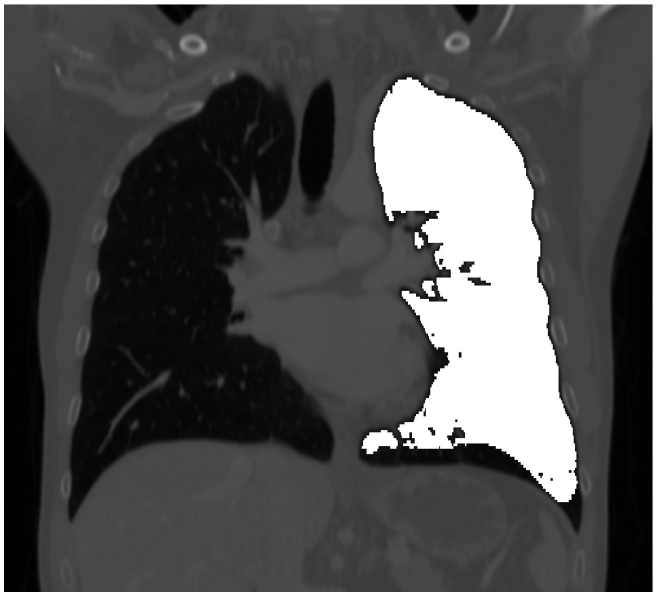

Figure 9: The result of running a simple region-growing segmentation algorithm using a computed seed point for the left lung is shown as a white area superimposed on the volume under examination.

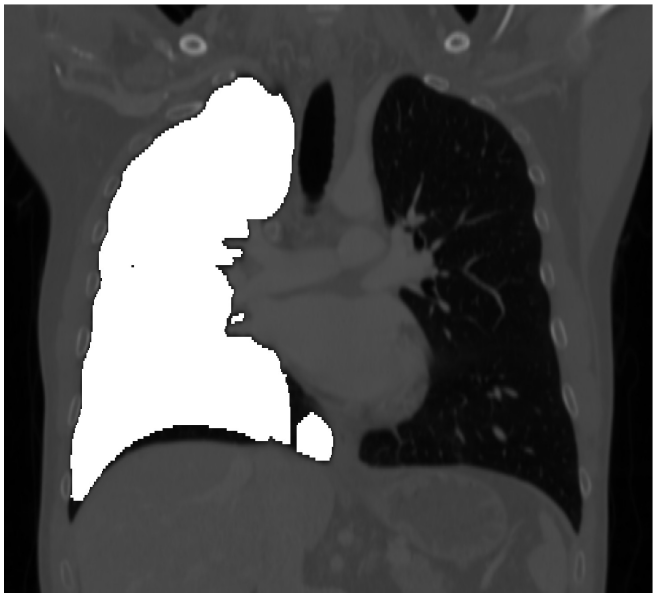

Figure 10: The result of running a simple region-growing segmentation algorithm using a computed seed point for the right lung is shown as a white area superimposed on the volume under examination.

4. DISCUSSIONS AND FUTURE WORK

This article presents a very generic, simple, and easy–to–implement approach to finding seed points for segmentation and eventual identification of any organ based on annotated 3D training data. Initial results indicate that it is indeed effective in finding seed points within the target organs and that a simple segmentation algorithm can subsequently delineate organs with a respectable degree of accuracy. It can be noted that the 3D probability maps themselves can be used as segmentations in areas where little contrast exists in the image itself or to transfer manual annotations from one modality such as CT to another modality such as MRI.

Despite the respectable Dice coefficients obtained above, it has to be noted that the segmentation will fail if the computed seed point happens to lie outside the target organ in volumes under examination. Thia can happen if such volumes belong to a patient whose body shape varies strongly from the body shapes in the training volumes. Examples of such a scenario include the segmentation of volumes of obese, extremely thin persons or children. Such an issue can be mitigated by deriving probability maps from a larger set of training images, which we intend to do in future work. In addition, we also intend to replace affine registration with an elastic registration method as this will allow the probability maps to overlap more closely with the organs for patients with extreme body shapes.

In addition, for organs having low contrast with their surroundings, segmentation is expected to be more challenging as it is difficult to find a discerning set of segmentation thresholds Th_L and Th_H. In such cases, the segmentation is liable to leak into tissue surrounding the target organ and that will lower the Dice coefficient and degrade the quality of the segmentation. Avoiding such leakage requires the development of a more sophisticated method to enhance the contrast between organs of interest and the voxels in their neighbourhoods.

Finally, owing to the limited size of the VISCERAL dataset, a limited set of results were presented. A more expansive set of results will be gathered as more data is acquired for testing the proposed method. This will include a more comprehensive study of the success rate of finding seed points falling within the confines of the target organ and the Dice coefficients for a large number of segmentation attempts.

5. CONCLUSIONS

The proposed method is a first but significant step towards achieving fully–automatic organ segmentation and identification based only on training data and that is, thus, well scalable. In this paper, it was demonstrated that

the computed seed points for region-growing segmentation do indeed lie within the target organs. In addition, it was demonstrated that even a simple segmentation algorithm can successfully delineate organs with a respectable degree of accuracy, as measured by Dice's coefficient.

However, some limitations to the approach do exist. It cannot be applied reliably to volumes belonging to patients having an extreme body shape as compared to the training data. The issue is due to the significantly large mismatch between the body–shape in the test volume and that in the reference volume. Nevertheless, the technique described in this paper is expected to perform well in all other cases. Future work will include modifications to the proposed approach that will increase the likelihood of successful segmentation for all body and organ shapes as well as for organs having low contrast with respect to the tissue surrounding them. It is expected that the proposed method will eventually play a significant role in the improvement in the way the ever–increasing mass of collected medical data is processed and stored.

6. ACKNOWLEDGEMENTS

This work was partially funded by the EU in FP7 in the context of the MD–Paedigree project (grant agreement 600932).

REFERENCES

1. Haux, R., "Hospital information systems — past, present, future," **75**, 268–281 (2005).
2. Müller, H., Zhou, X., Depeursinge, A., Pitkanen, M., Iavindrasana, J., and Geissbuhler, A., "Medical visual information retrieval: State of the art and challenges ahead," in [*Proceedings of the 2007 IEEE International Conference on Multimedia and Expo*], *ICME'07*, 683–686, IEEE (July 2007).
3. Langs, G., Müller, H., Menze, B. H., and Hanbury, A., "Visceral: Towards large data in medical imaging — challenges and directions," *Lecture Notes in Computer Science* **7723**, 92–98 (2013).
4. Berger, M., [*Geometry. I. Universitext*], Springer-Verlag, Berlin (1987).
5. Cover, T. M. and Thomas, J. A., "Entropy, relative entropy and mutual information," *Elements of Information Theory* , 12–49 (1991).
6. Mattes, D., Haynor, D. R., Vesselle, H., Lewellen, T. K., and Eubank, W., "Nonrigid multimodality image registration," *Medical Imaging* **4322**(1), 1609–1620 (2001).
7. Mattes, D., Haynor, D. R., Vesselle, H., Lewellen, T. K., and Eubank, W., "Pet-ct image registration in the chest using free-form deformations," *IEEE Transactions on Medical Imaging* **22**(1), 120–128 (2003).
8. Unser, M., Aldroubi, A., and Eden, M., "B-spline signal processing. i. theory," *IEEE Transactions on Signal Processing* **41**(2), 821–833 (1993).
9. Unser, M., Aldroubi, A., and Eden, M., "B-spline signal processing. ii. efficiency design and applications," *IEEE Transactions on Signal Processing* **41**(2), 834–848 (1993).
10. Unser, M., "Splines: A perfect fit for signal and image processing," *IEEE Signal Processing Magazine* **16**(6), 22–38 (1999).
11. Hummel, R., "Image enhancement by histogram transformation," *Computer Graphics and Image Processing* **6**(2), 184 – 195 (1977).
12. Perona, P. and Malik, J., "Scale-space and edge detection using anisotropic diffusion," *Pattern Analysis and Machine Intelligence, IEEE Transactions on* **12**(7), 629–639 (1990).
13. Dice, L. R., "Measures of the amount of ecologic association between species," *Ecology* **26**(3), 297–302 (1945).
14. Fedorov, A., Beichel, R., Kalpathy-Cramer, J., Finet, J., Fillion-Robin, J.-C., Pujol, S., Bauer, C., Jennings, D., Fennessy, F., Sonka, M., et al., "3d slicer as an image computing platform for the quantitative imaging network," *Magnetic Resonance Imaging* (2012).